Atmos. Chem. Phys. Discuss., 14, 8015–8061, 2014
www.atmos-chem-phys-discuss.net/14/8015/2014/
doi:10.5194/acpd-14-8015-2014

Atmospheric Chemistry and Physics Discussions

Air–sea fluxes of oxygenated volatile organic compounds across the Atlantic Ocean

M. Yang[1], R. Beale[1], P. Liss[2,3], M. Johnson[2,4], B. Blomquist[5], and P. Nightingale[1]

[1]Plymouth Marine Laboratory, Prospect Place, Plymouth, UK
[2]School of Environmental Sciences, University of East Anglia, Norwich, UK
[3]Department of Oceanography, Texas A & M University, College Station, TX, USA
[4]Centre for Environment, Fisheries and Aquaculture Science, Lowestoft, UK
[5]Department of Oceanography, University of Hawaii, Honolulu, HI, USA

Received: 4 March 2014 – Accepted: 13 March 2014 – Published: 24 March 2014

Correspondence to: M. Yang (reelguy@gmail.com)

Published by Copernicus Publications on behalf of the European Geosciences Union.

Abstract

We present air–sea fluxes of oxygenated volatile organics compounds (OVOCs) quantified by eddy covariance during the Atlantic Meridional Transect cruise in 2012. Measurements of acetone, acetaldehyde, and methanol were made in several different oceanic provinces and over a wide range of wind speeds of 1–18 $m s^{-1}$. The ocean appears to be a sink for acetone in the higher latitudes of the North Atlantic but a source in the subtropics. In the South Atlantic, seawater acetone was near saturation relative to the atmosphere, resulting in essentially zero net flux. For acetaldehyde, a small oceanic emission is implied from measured flux, but of a lower magnitude than predicted based on the two-layer model. Chemical enhancement of air–sea acetaldehyde exchange due to aqueous hydration appears to be minor. The deposition velocity of methanol correlates linearly with the transfer velocity of sensible heat, confirming predominant airside control. We examine the relationships between the OVOC concentrations in air as well as in water, and compute the gross emission and deposition fluxes of these gases.

1 Introduction

Oxygenated Volatile Organic Compounds (OVOCs) including acetone, acetaldehyde, and methanol are present ubiquitously in the lower atmosphere. The sum of these three gases accounted for 37–63 % of the total (non-methane) observed organic carbon (gaseous and particulate) in marine air (Heald et al., 2008). OVOCs influence the tropospheric oxidative capacity and air quality by influencing the cycling of ozone and the hydroxyl radical (Carpenter et al., 2012). In the surface ocean, dissolved OVOCs represents a source of energy and carbon for microbes (Dixon et al., 2013). Dachs et al. (2005) estimated a large air-to-sea flux of gaseous total organic carbon (TOC) in the Northeast Subtropical Atlantic (tens of $mmol\,m^{-2}\,d^{-1}$), often similar in magnitude to the CO_2 flux. Here we quantify the net air–sea transport of acetone, acetaldehyde, and methanol, which are uncertain in not only magnitude, but also in direction.

ACPD
14, 8015–8061, 2014

Terrestrial plant emissions and atmospheric oxidation of precursors are the main sources of atmospheric acetone in the global budget by Fischer et al. (2012). Estimates of the magnitude and direction of the air–sea acetone flux vary. Jacob et al. (2002) suggested that acetone is removed from the marine boundary layer by deposition to the sea surface and subsequent microbial consumption ($-14\,\mathrm{Tg\,yr^{-1}}$), and produced by photolysis of dissolved organic matter in surface waters ($27\,\mathrm{Tg\,yr^{-1}}$), yielding a net oceanic source of $13\,\mathrm{Tg\,yr^{-1}}$. Singh et al. (2004) modeled an oceanic source of $80\,\mathrm{Tg\,yr^{-1}}$, which is negated by deposition to yield a net loss of $-14\,\mathrm{Tg\,yr^{-1}}$ to the surface ocean. Based on eddy covariance (EC) measurements (with atmospheric pressure ionization mass spectrometry) over the Pacific, Marandino et al. (2005) estimated a net deposition loss of $-48\,\mathrm{Tg\,yr^{-1}}$ globally. Other observations at sea (Taddei et al., 2009; Beale et al., 2013) indicate the air–sea net flux of acetone to be small and variable in sign temporally as well as spatially.

Terrestrial plants, atmospheric oxidation of precursors, and the surface ocean are all sources of atmospheric acetaldehyde (Guenther et al., 2000; Jardine et al., 2008; Millet et al., 2010). Based on air concentration measurements over the Pacific, Singh et al. (2003) estimated an oceanic emission of $125\,\mathrm{Tg\,yr^{-1}}$. Combining colored dissolved organic matter (CDOM) derived from satellite and laboratory acetaldehyde production rate, Millet et al. (2010) modeled an oceanic emission of $57\,\mathrm{Tg\,yr^{-1}}$. From in situ seawater concentrations, Beale et al. (2013) calculated a much lower oceanic emission (mean of $17\,\mathrm{Tg\,yr^{-1}}$) than those earlier estimates. These discrepancies are partly due to different treatments of chemical enhancement in the computation of air–sea acetaldehyde exchange (see Sect. 4.2). To our knowledge, the air–sea flux of acetaldehyde has never been directly measured over the open ocean.

Atmospheric methanol mainly originates from terrestrial plants, with additional contributions from biomass and biofuel burning, industrial emissions, and atmospheric oxidation of precursors (Guenther et al., 2000; Singh et al., 2000; Heikes et al., 2002; Jacob et al., 2005; Millet et al., 2008). Methanol is mostly removed from air by photochemical destruction, deposition to land (Karl et al., 2004) and to the ocean surface (Heikes

ACPD
14, 8015–8061, 2014

et al., 2002; Williams et al., 2004; Carpenter et al., 2004). Based on in situ seawater concentrations in the Atlantic, Beale et al. (2013) estimated both positive and negative air–sea fluxes, with a mean net oceanic emission of 12 $Tg\,yr^{-1}$. From the cruise detailed in this paper, Yang et al. (2013b) measured a net atmospheric deposition of methanol into the ocean by EC that extrapolates to $-42\,Tg\,yr^{-1}$ globally. The discrepancy in these estimates illustrates the large uncertainties remaining in our understanding of methanol cycling.

On the 22nd Atlantic Meridional Transect (AMT-22) cruise from Southampton, UK to Punta Arenas, Chile in 2012 on the Royal Research Ship *James Cook*, we directly measured the air–sea fluxes of acetone, acetaldehyde, and methanol by EC with a high sensitivity proton-transfer-reaction mass spectrometer (PTR-MS, Ionicon Analytik, Austria). The results for methanol have been published previously (Yang et al., 2013b); we include them here for completeness of the data set, as well as to explain the methodology in more detail and compare the relationships between the three gases. The PTR-MS, first described by Lindinger et al. (1998), uses hydronium ions (H_3O^+) to protonate analytes present in the drift tube, which are subsequently detected by quadrupole mass spectrometry. This soft form of ionization results in little or no fragmentation of the parent molecule. In recent years the PTR-MS has been used with the EC method to measure the vertical fluxes of OVOCs at terrestrial sites (e.g. Karl et al., 2001; Yang et al., 2013a). Compared to land based measurements, the application of EC on a ship is challenged by motion-induced artifacts as well as generally lower fluxes. Our effort here, to the best of our knowledge, represents the first utilization of the PTR-MS for EC flux measurements at sea. We also measured the concentrations of these compounds in seawater with the same PTR-MS as used for the atmospheric measurements coupled to a membrane inlet (described by Beale et al., 2011). This allows us to directly compare EC fluxes with predicted values based on gas transfer parameterizations (Appendix A).

ACPD
14, 8015–8061, 2014

2 Experimental

The sampling track of AMT-22 cruise is shown in Fig. 1, color-coded by chlorophyll *a* concentration (measured by fluorescence and verified by absorption) and marked on selected dates. The annual voyage (www.amt-uk.org) contributes to a long-term time series of biological, chemical, and physical oceanographic parameters across the Atlantic and allows us to examine the magnitude and variability of air–sea OVOC exchange across different oceanic regions.

2.1 Atmospheric OVOC concentrations (C_a)

The PTR-MS was located in the meteorological laboratory near the foredeck of the ship. All data (concentration, wind, motion, flow) were logged on the same computer, which was synchronized to the GPS clock daily. For ~ 19 h of a day, the PTR-MS sampled ambient air drawn into the laboratory by a vacuum pump from the meteorological platform above ship's bow (z = 18 m a.m.s.l.) via ~ 25 m of 6.4 mm ID Teflon PFA tubing. The fully turbulent manifold flow (~ 23 standard liters per minute, Reynolds number of ~ 5000) was recorded by a digital thermal mass flow meter (Bronkhorst EL-FLOW series). Nominal settings of the PTR-MS were: drift chamber temperature of 80 °C, voltage of 700 V, and source water vapor flow of 9 standard cubic centimeter per minute (sccm). Instrument sensitivity typically increased with the chamber pressure, which was regulated such that the m/z 37 signal ($H_2OH_3O^+$) remained less than 5–6 % of the source ion (H_3O^+) signal. This pressure varied from 2.8 mbar in higher latitudes to 2.5 mbar in the tropics due to changes in ambient humidity. The m/z 32 (O_2^+) signal was ~ 1 % of the source ion signal, which averaged ~ 2.5×10^7 counts per second (cps) during the cruise.

Continuous internal isotopic standards were used to account for changes in reaction rates and transmission efficiencies in the PTR-MS. Deuterated methanol (d_3-methanol, with protonated mass to charge ratio m/z of 36) and acetone (d_6-acetone, m/z of 65) gas standards in nitrogen (2.0 ± 0.1 ppm, Scientific and Technical Gases Ltd) were

ACPD
14, 8015–8061, 2014

injected continuously into the manifold at ~2 m ahead of the subsampling "tee" for the PTR-MS. The standard flow was regulated by a digital thermal mass flow controller (Bronkhorst EL-FLOW series) at 30(±0.3) sccm, resulting in diluted standard concentrations of ~2.6 ppb. The main tubing was wrapped with opaque insulating foam to prevent photochemistry and condensation of water in the interior wall.

For most of the cruise, methanol (m/z 33), acetaldehyde (m/z 45), and acetone (m/z 59) were measured under multiple ion detection (MID) mode. The PTR-MS cycled through m/z 21 ($H_3^{18}O^+$, dwell time of 50 ms), 33 (100 ms), 36 (50 ms), 45 (100 ms), 59 (100 ms), and 65 (50 ms) with total sampling frequency of ~2.1 Hz. Between 3 November and 16 November, we chose to measure atmospheric acetaldehyde for only ~2 h a day (near the times of the CTD casts) because of its low ambient abundance. We also monitored the concentrations of isotopic standards, $H_2OH_3O^+$, and O_2^+ from daily scans. The gas standards were stable over the duration of the cruise.

The derivation of atmospheric methanol concentration from isotopic standard addition is detailed by Yang et al. (2013a, b). The ambient concentration of atmospheric acetone (C_{acetone}) is analogously:

$$C_{\text{acetone}} = C_{\text{acetone,std}} \frac{(\text{cnts}_{59}/\text{cnts}_{65})A_{65,\text{std}} - A_{59,\text{std}}}{A_{59,\text{amb}}} \quad (1)$$

Here $C_{\text{acetone, std}}$ is the concentration of d_6-acetone; cnts_{59} and cnts_{65} are the signals at m/z 59 and 65 after subtracting the backgrounds (see Appendix B for discussion on backgrounds). Mass scans indicates $A_{65,\text{std}}$, the isotopic ratio of m/z 65 in the gas standard, to be 0.86; we adjust this value to 0.90 to account for the ~4 % higher transmission efficiency expected at m/z 65 than at m/z 59. The standard gas cylinder contains a small amount of undeuterated acetone, which is represented by $A_{59,\text{std}}$ (~0.02 from mass scans). At 0.96, $A_{59,\text{amb}}$ is the isotopic ratio of m/z 59 in ambient air from natural abundance of elements. The abundance of the deuterated isotopomer in ambient air is insignificant and neglected in this analysis.

ACPD
14, 8015–8061, 2014

Because of the unit mass resolution of the PTR-MS, propanal and glyoxal are not distinguished from acetone at m/z 59. Singh et al. (2004) reported ~ 0.07 ppb of propanal for the lowest 2 km of the remote tropical Pacific. The low concentration is consistent with its predominant anthropogenic origin and short atmospheric lifetime. From satellite measurements in the UV-visible range, Stavrakou et al. (2009) and Lerot et al. (2010) retrieved a glyoxal column concentration of $1–4\times10^{14}$ molecules cm^{-2} over the Atlantic in the Northern Hemisphere autumn. Even assuming all of the glyoxal is contained within a well-mixed, 1 km marine atmospheric boundary layer, this corresponds to an approximate mixing ratio of 0.03–0.12 ppb at ambient temperatures, of the same order as shipboard glyoxal measurements by Sinreich et al. (2010) from the southeast Pacific and a few times lower than typical acetone levels. Moreover, glyoxal is probably not ionized efficiently in the PTR-MS due to its low proton affinity (Wróblewski et al., 2007). During AMT-22, predicted fragment ions of propanal and glyoxal were examined with a separate GC-MS system in both air and water of the subtropical North Atlantic but not clearly detected (S. Hackenberg, personal communication, 2012). Nevertheless, measured atmospheric acetone concentrations may be upper limits due to these potential interferences.

The atmospheric acetaldehyde concentration from this cruise is more uncertain due to the lack of a suitable standard, which tends to be unstable in both gas cylinders and permeation devices. We used the low pass filtered source ion count at m/z 21, the average kinetic reaction rate presented by Zhao and Zhang (2004), and instrument-specific transmission efficiencies to compute its concentrations. As with Yang et al. (2013a), we further adjust the derived acetaldehyde concentration by the ratio between ambient methanol concentration determined from isotopic dilution and the direct output of the instrument ($C_{\text{methanol}}/C_{33,\text{PTR-MS}}$). The detection limits for mean atmospheric concentrations (2 min average) for acetone, and acetaldehyde, and methanol were about 0.02, 0.02, and 0.05 ppb, respectively.

A plastic funnel, initially attached to the front of the gas inlet to keep out water droplets, was unexpectedly found to emit compounds at m/z 45 and 59. Exposed

ACPD
14, 8015–8061, 2014

to sunlight for six months continuously prior to this cruise, the funnel appeared to have photochemically degraded over time. Emissions from the funnel were not obvious at the beginning of the cruise under overcast and cool (< 15 °C) conditions, but became increasingly pronounced when the ship approached the tropics. Contamination was more severe under direct sunlight and high temperatures than at night, leading to unrealistic diurnal cycles in acetone and acetaldehyde concentrations (Fig. 2). Methanol was not affected. The funnel was removed from the inlet on 29 October (~ 5° N) and the problem disappeared immediately thereafter. However, atmospheric acetone and acetaldehyde data before 29 October were highly uncertain. We discard their daytime concentrations during that period and crudely correct the nighttime data for funnel induced artifacts by detrending the concentrations with respect to air temperature.

2.2 Seawater OVOC concentrations (C_w)

Discrete seawater samples were taken from predawn and noontime CTD casts daily. At each station, triplicate seawater samples were collected from the 5 m Niskin bottle via a short piece of Tygon™ tubing into opaque glass bottles to prevent alteration to OVOC concentrations via photochemical reactions. Air contamination was avoided by sampling first from the Niskin, taking care to avoid bubbling, and overfilling the glass bottles for several seconds before capping. To minimize modification of OVOC concentrations by biological activity, water samples were analyzed within 3 h of collection. OVOCs were extracted from seawater across a semi-permeable silicone membrane thermostated at 50 °C into a supply of cleaned nitrogen gas flowing directly into the PTR-MS. The first of the triplicates at each station was used to condition the membrane. Reported seawater OVOC concentrations represent the averages of the latter two replicates, which generally agreed within the noise level. Calibration slopes were determined approximately every two weeks from equivalent analyses of aqueous standards, which were freshly prepared by serial dilution of reagent-grade methanol, acetone, and acetaldehyde. The calibration slopes were consistent over the entire cruise, generally varying by less than 10 %.

ACPD
14, 8015–8061, 2014

We also took water samples from the deepest Niskin bottle (~ 500 m depth) at noon each day. The precisions of the seawater measurements were estimated from 3 standard deviation (σ) of eight replicate 500 m samples collected on 20 November. For methanol, acetaldehyde, and acetone the precisions were 11, 0.6, and 1.8 nM, which represent 38, 11, and 13 % of the mean concentrations of these compounds. In comparison, 3σ of the instrument backgrounds of these eight replicates (i.e. measuring cleaned nitrogen gas) were 6, 0.3, and 0.3 nM. All OVOC concentrations measured during AMT-22 were above these detection limits.

3 Eddy covariance setup and flux computations

A 3-D sonic anemometer (WindMaster, Gill) measuring wind velocities and a 6 degree of freedom motion sensor (Motionpak II, Systron Donner) measuring linear accelerations and rotational rates were installed 40 cm from the air intake. To minimize wind disturbance by the ship's searchlight mounted in the middle, the sensors and inlet were positioned on the starboard side of the meteorological platform and rotated 44° from the bow. Motion data were measured at ~ 15 Hz and later interpolated to match the frequency of winds (10 Hz).

Aside from stopping for twice-a-day CTD casts, the ship steamed steadily at a regular speed and heading. After discarding occasional periods of excessive ship maneuvering (e.g. changing speed or heading), hourly wind/motion data were processed following Edson et al. (1998) to yield true winds (u, v, w). Further sequential decorrelations of corrected winds with ship velocities and accelerations removed residual motion cross-correlation (Fairall et al., 2000). The resultant motion-corrected wind velocities were used in the hourly EC computations of OVOC fluxes ($\overline{w'\mathrm{OVOC}'}$), sensible heat flux ($Q_\mathrm{H} = \overline{w'T'_\mathrm{a}}$), and momentum flux ($\tau = \rho\overline{w'u'}$). Here T_a is the sonic temperature corrected for humidity and ρ is air density.

ACPD
14, 8015–8061, 2014

3.1 OVOC flux processing

A lag correlation analysis was performed hourly between OVOC and w to determine the delay in atmospheric concentrations relative to wind. The most consistent lag time (~ -5.5 s) was determined from the methanol analysis due to its larger flux magnitude than other OVOCs. This delay is consistent with the expected transit time in the main inlet (~ 2 s) and subsampling line followed by reaction chamber (~ 3 s). After synchronization, the OVOC fluxes were computed from the integral of the $C_a : w$ cospectrum from 0.002 to 1 Hz.

To examine the contributions from different frequencies to the turbulent flux, in Fig. 3 we show the cospectra of methanol, acetaldehyde, acetone, sensible heat, and momentum averaged over 10 h on 16 October ($\sim 35^\circ$ N), a day of fairly high winds ($13\,\mathrm{m\,s^{-1}}$) and moderate swell (vertical platform variance of $\sim 1\,\mathrm{m^2\,s^{-2}}$). Each spectrum has been normalized by the respective flux magnitude, preserving the original sign convention. The heat, momentum, and methanol cospectra all demonstrate the expected spectral shape for atmospheric turbulent transfer (Kaimal et al., 1972). In rougher seas, some motion-sensitivity is apparent in the methanol flux, which has been corrected with a decorrelation method (Appendix C). The acetone cospectrum is fairly well defined during this period except for some loss of signal above ~ 0.1 Hz. The acetaldehyde cospectrum is much noisier and demonstrates large distortions above ~ 0.2 Hz, likely related to emissions from the plastic funnel (Appendix D). We also considered the potential contributions to OVOC fluxes due to fluctuations in air density (i.e. Webb et al., 1980), which are insignificant (Appendix E).

With increasing wind speed, the turbulent cospectrum shifts towards higher frequencies, resulting in a greater OVOC flux loss as a result of the limited sampling rate (~ 2.1 Hz). Yang et al. (2013a) quantified the high frequency flux attenuation of this system using the Ogive approach (by comparison with the concurrent sensible heat flux, Spirig et al., 2005) and the filter function approach (based on the instrumental response time, Bariteau et al., 2010), which led to similar results. The low signal to

ACPD
14, 8015–8061, 2014

noise in both OVOC and sensible heat flux over the ocean limits the usefulness of the Ogive approach. Due to noise in the individual cospectrum, applying the filter function hourly tends to amplify the scatter in the flux. Instead, we first apply the filter function inversely to theoretical cospectra (Kaimal et al., 1972) calculated at wind speeds of 2–18 $m s^{-1}$. The ratio between the integrals of the Kaimal cospectra and the artificially attenuated cospectra up to the Nyquist frequency yield an effective flux correction factor as a function of wind speed. We further account for the small flux contribution above the Nyquist frequency (usually a few percent) by scaling to the full Kaimal cospectra. The total flux loss ranged from ~ 10 % to 16 % to 21 % at wind speeds of 5, 10, and 15 $m s^{-1}$, respectively.

3.2 Quality control filters for EC

We limit the relative wind sector to −50–110° and the relative wind speed to > 2 $m s^{-1}$ for flux measurements to avoid airflow distortion from the ship's superstructure and searchlight, as well as contamination in OVOC signals from the ship's exhaust. Hourly constraints for ship maneuvers and the homogeneity/stationarity conditions assumed by EC include σ of relative wind direction less than 80°, σ of true wind speed less than 2 $m s^{-1}$, and σ of w less than 1 $m s^{-1}$. We compute hourly heat fluxes from the integral of the $T_a : w$ cospectrum over the entire frequency range (0.00033–5 Hz) as well as over 0.002–5 Hz. Additional heterogeneity/nonstationarity is identified when Q_H calculated from these two frequency ranges differ by more than 30 %, which occurred ~ 10 % of the time over the entire cruise. Overall, ~ 70 % (584 h) of sensible heat and momentum fluxes satisfied these criteria.

For OVOCs, to satisfy homogeneity/stationarity we also omitted periods when the hourly trends in methanol, acetone, and acetaldehyde were greater than 0.2, 0.1, and 0.04 ppb h^{-1}, respectively, which occurred ~ 10 % of the time. In the cases of acetone and acetaldehyde, we also discarded hours when the respective σ exceeded 0.3 and 0.2 ppb to limit the effect of contamination from the plastic funnel at the front of the

ACPD
14, 8015–8061, 2014

intake. The number of hours that satisfied all of the requirements above was 484, 310, and 218 for methanol, acetone, and acetaldehyde, respectively.

3.3 OVOC flux detection limits and uncertainties

Uncertainty in OVOC flux measurements is a function of both random noise and natural variance in the chemical signal (Blomquist et al., 2010). We estimate the detection limit for hourly flux measurement as 3σ of the covariance function at an implausible lag time between OVOC and w (+15 s) during periods of fairly steady winds and OVOC concentrations. Over 16 h from 31 October to 1 November, with a wind speed of $\sim 10\,\mathrm{m\,s^{-1}}$, the hourly detection limits were ~ 10, 4, and $5\,\mu\mathrm{mol\,m^{-2}\,d^{-1}}$ for methanol, acetaldehyde, and acetone. Random uncertainty in the EC flux may be reduced by averaging to one-degree latitude bins ($\propto N^{-1/2}$, where N is the number of independent measurements). At a ship speed of $18\,\mathrm{km\,h^{-1}}$, each latitude bin is traversed in ~ 6 h, implying that the detection limits of these compounds were ~ 4, 2, and $2\,\mu\mathrm{mol\,m^{-2}\,d^{-1}}$ for the latitudinal averages. By this definition, ~ 90 % of the latitudinally averaged methanol flux exceeded the detection limit. For acetone, this percentage was ~ 80 % for the Northern Hemisphere and only ~ 10 % for the Southern. For acetaldehyde, the measured flux was above detection limit only ~ 30 % of the time for the entire transect.

Estimated following Blomquist et al. (2010) with the empirical constant a set to 1, hourly sampling uncertainty was 30–40 % and 60–140 % for methanol and acetone flux, respectively (greater in Southern Hemisphere as a result of the lower flux magnitude). Because the EC acetaldehyde flux approaches zero, the relative flux uncertainty for this compound is even greater. We estimate the contribution to total flux uncertainty from instrumental noise to be about 40, 60, and 80 % for methanol, acetone, and acetaldehyde during the period from 31 October to 1 November. Between 3 November and 16 November, the dwell time at m/z 33 was doubled to 200 ms to compensate for the lower atmospheric methanol concentration (and natural variance) in the South Atlantic, which reduced the hourly detection limit to $\sim 6\,\mu\mathrm{mol\,m^{-2}\,d^{-1}}$ for this compound.

ACPD
14, 8015–8061, 2014

Among the three OVOCs, improving sensitivity and reducing noise of the instrument would have the greatest benefit for the detection of acetaldehyde flux.

4 Results and discussion

Figure 4 shows the latitudinal distributions of sea surface temperature (SST), air temperature (T_a), salinity, momentum flux (τ), 10 m neutral wind speed, sensible heat flux (Q_H), and the sea–air temperature difference (ΔT). Scaled approximately to the square of the wind speed, τ peaked during the high winds at ~ 36° N and ~ 33° S. Sensible heat flux, in comparison, was driven by both wind speed and ΔT. Within the Inter Tropical Convergence Zone (ITCZ) where ΔT was large, Q_H remained low because of the low winds. The Monin–Obukhov stability parameter (z/L) from the COARE model (Fairall et al., 2011) was negative for majority of the cruise, indicating an unstable atmosphere. In high latitude regions and during short periods preceding storms, z/L became slightly positive (weakly stable), due to warm air from frontal passages advecting over cold water. We normalize the transfer velocities of heat ($k_{heat} = Q_H/\Delta T$) as well as methanol (Sect. 4.3) to neutral stability based on similarity theory (Fairall et al., 1996). This assumes that heat and methanol have the same stability function (ψ) as water vapor, which was computed from COARE. As the marine atmosphere was usually unstable, normalizing to neutral stability reduces the transfer velocities by ~ 8 % on average.

Measured and predicted k_{heat} from COARE generally agree (Fig. 5). Three averaging schemes of the EC data are shown: hourly Q_H divided by hourly ΔT, bin-average of hourly k_{heat} according to wind speeds (error bars indicate 1 α), and latitudinally averaged Q_H divided by latitudinally averaged ΔT. There is no obvious bias between the latter two averaging methods, as would be expected from a relatively linear relationship of k_{heat} with wind speed. Compared to hourly data, reduction in scatter in the averaged results can be attributed to cancellation of random errors. As shown already by Yang et al. (2013b), the measured friction velocity, $u_* = (-\tau/\rho)^{1/2}$, matches well

ACPD
14, 8015–8061, 2014

with prediction from COARE. The consistencies in measured and modeled momentum/sensible transfer validate the motion correction.

Now we turn our attention to OVOCs. For comparison, we frequently refer to the works by Beale et al. (2013). They measured the seawater concentrations of methanol, acetone, and acetaldehyde along the same transect and during the same months three years prior (AMT-19) using the identical PTR-MS/membrane inlet system, and also estimated the air–sea fluxes based on modeled atmospheric concentrations.

4.1 Acetone

Figure 6a shows the latitudinal distributions of acetone concentrations in air and in near-surface water. Displaying a distinctive hemispheric trend, atmospheric acetone concentrations were ~ 0.6, 0.4, and 0.2 ppb in the North, Equatorial, and South Atlantic, similar to previous measurements by Lewis et al. (2005), Williams et al. (2004), and Taddei et al. (2009), respectively. C_a peaked in the subtropical North Atlantic at ~ 0.9 ppb, within range of a five-year record at Cape Verde (Read et al., 2012) and shipboard observations by Marandino et al. (2005) in the Pacific at similar latitudes. With a mean value of 13.7 nM, dissolved acetone concentration is also consistent with previous open ocean observations (e.g. Williams et al., 2004; Marandino et al., 2005; Kameyama et al., 2010). In particular, C_w distribution from this cruise shows remarkable similarity to measurements by Beale et al. (2013) during AMT-19.

Seawater acetone concentration peaked at 36 nM in the oligotrophic North Atlantic subtropical gyre, where Chl *a* concentration was low ($< 0.1\ \mu g\,L^{-1}$). South of 32° S, C_w was only ~ 5 nM despite high biological productivity (Chl $a > 1\ \mu g\,L^{-1}$). Photochemical destruction of DOM is thought to be a source of acetone (Dixon et al., 2013; Kieber et al., 1990; Zhou and Mopper, 1997). Seawater acetone concentration measured from 500 m was typically 20–40 % of 5 m value (Fig. 7), consistent with production predominantly in the photic layer. Similar depth profiles were observed by Williams et al. (2004) and Beale et al. (2013). Despite the expected photochemical source, seawater acetone concentrations from predawn and solar noon casts were statistically identical in

ACPD
14, 8015–8061, 2014

our measurements. C_w also did not demonstrate a positive correlation with CDOM measured on this cruise (G. Tilstone, AMT-22 Cruise Report). Such light-driven effects might become more obvious at a depth shallower than 5 m.

For most of the cruise, the atmospheric and seawater acetone concentrations followed relatively similar distributions. Significant deviations from equilibrium were observed north of 40° N, where the surface ocean was undersaturated, and in the North Atlantic subtropics, where the ocean was supersaturated (Fig. 6b), in agreement with Beale et al. (2013). Calculated saturation levels were noisy south of 32° S partly due to low atmospheric concentrations (~ 0.1 ppb). Interestingly, acetone was nearly 100 % saturated in the Southern Hemisphere, which suggests the oceanic production and consumption rates of this compound in that region were strongly coupled and/or relatively slow, such that air–sea exchange could maintain equilibrium. A slow removal rate would be consistent with the long oceanic lifetime of acetone (5–55 days) recently reported by Dixon et al. (2013).

Measured and predicted air–sea acetone fluxes are in broad agreement and consistent with saturation values (Fig. 6c). The saturation state and the sign of predicted flux become more sensitive to the choice of solubility the closer the compound is to equilibrium. For example, from 12° N to 3° N, a mean acetone flux $-0.6\,\mu mol\,m^{-2}\,d^{-1}$ is predicted using the solubility from Zhou and Mopper (1990). If the solubility from Benkelberg et al. (1995) is used instead, the predicted flux becomes $1.0\,\mu mol\,m^{-2}\,d^{-1}$. We also examine the sensitivity of the predicted flux with respect to the choice of k_a. For simplicity, if we take the measured methanol deposition velocity (Sect. 4.3) to be k_a for acetone, the magnitude of the predicted acetone flux would be ~ 10 % higher than what is shown in the subtropical North Atlantic. Uncertainties in the acetone flux and atmospheric concentration were large in the North Atlantic due to the funnel contamination, while flux was near zero in the South Atlantic. Thus we are unable derive a reliable total transfer velocity of acetone.

Taddei et al. (2009) suggested enhanced acetone emission in regions of phytoplankton blooms based on highly uncertain flux measurements (in part due to a lack of

ACPD
14, 8015–8061, 2014

motion correction on winds). Similar to Beale et al. (2013), we observed neither greater emission nor elevated acetone concentration in biologically productive waters. Over the entire transect, the emission and deposition fluxes of acetone largely cancel, resulting in mean (standard error) EC flux of −0.2 (0.4) $\mu mol\,m^{-2}\,d^{-1}$ and predicted flux of 1 (0.4) $\mu mol\,m^{-2}\,d^{-1}$. The discrepancy between these two different estimates suggests additional uncertainties that are not accounted for by the standard error. Crudely extrapolating to the total area of the world oceans (assuming the same concentrations, wind speeds, temperatures, etc as during AMT-22), the net air–sea acetone transport inferred from EC and predicted fluxes is −1 (3) and 8 (3) $Tg\,yr^{-1}$, respectively. These estimates are similar in magnitude to modeled results from Fischer et al. (2012) as well as extrapolations by Beale et al. (2013).

4.2 Acetaldehyde

Figure 8a shows the latitudinal distributions of acetaldehyde in air and near-surface water. Atmospheric acetaldehyde concentration averaged ∼ 0.18 ppb in the Northern Hemisphere, within the range of previously measured values in the arboreal autumn (e.g. Lewis et al., 2005; Read et al., 2012). A peak in C_a at ∼ 10° N (∼ 0.25 ppb) mirrored the peaks in the concentrations of acetone and methanol, in the outflow region of North Africa. C_a was lower in the Southern Hemisphere, with an average of ∼ 0.08 ppb. Seawater acetaldehyde decreases from ∼ 9 nM in the higher latitude North Atlantic to ∼ 4 nM in the South Atlantic. These C_w values are within the range of previous seawater measurements (Mopper and Kieber, 1991; Zhou and Mopper, 1997; Beale et al., 2013).

Statistically there was no difference between noon (5.5 ± 1.7 nM) and predawn (5.2 ± 1.7 nM) values for surface acetaldehyde, similar to the findings of Beale et al. (2013). This is in contrast to Zhou and Mopper (1997), who reported enrichment in the microlayer of calm and presumably productive Florida waters compared to bulk water and attributed it to photochemical production. As with acetone, seawater acetaldehyde concentration did not demonstrate a positive relationship with CDOM (G. Tilstone, AMT-22 Cruise Report). Acetaldehyde concentration at ∼ 500 m was similar to the near surface

ACPD
14, 8015–8061, 2014

(Fig. 7), consistent with depth profiles observed by Mopper and Kieber (1991) in the Black Sea and Beale et al. (2013) from AMT-19. The absences of a significant diel cycle as well as a vertical gradient are consistent with the results from Dixon et al. (2013), who reported a rapid microbial sink of acetaldehyde in surface seawater (lifetime < 1 d) that strongly controls its surface concentration.

Acetaldehyde appears to be significantly supersaturated in seawater relative to the atmosphere through out the Atlantic (average saturation of ~ 300 %, Fig. 8b), implying consistent emission. Dissolved acetaldehyde exists in equilibrium with the hydrate 1,1-ethanediol, $CH_3CH(OH)_2$, with a hydration constant (ε) of around 1.4 (Bell and Avans, 1966). Only the unhydrated form is volatile and directly subject to air–sea exchange. Since our measurements are calibrated using aqueous standards diluted from pure acetaldehyde, they represent total concentration in water ($CH_3CHO + CH_3CH(OH)_2$). The same is true with earlier HPLC techniques (e.g. Zhou and Mopper, 1990, 1997).

The reversible hydration/dehydration reaction rate constant is of the order of $\sim 0.1\,s^{-1}$ at 25 °C and a pH of 8.1 (Bell et al., 1956; Kurz and Coburn, 1967). Because of this relatively rapid rate, solubility of acetaldehyde reported in the literature usually represents the apparent solubility (H^*), corresponding to the ratio between total dissolved acetaldehyde and the gas phase concentration. H^* is related by the factor of $1/(1+\varepsilon)$ to the intrinsic Henry's solubility (H) between dissolved CH_3CHO and the gaseous constituent. The hydration reaction increases the effective rate of aqueous diffusion (D), and so reduces waterside resistance in air–sea transfer. Using the equilibrium hydration constant from Bell and Avans (1966), hydration rate from Schecker and Schultz (1969), and the thickness of the aqueous diffusive sub-layer (D/k_w), Zhou and Mopper (1997) estimated a chemical enhancement factor (A) of 2 for acetaldehyde using the model from Hoover and Berkshire (1969).

We calculate acetaldehyde flux following Eqs. (A1) and (A2), but with H^* in place of H. To demonstrate the effect of chemical enhancement, flux is computed with $A = 1$ (no enhancement, e.g. Beale et al., 2013) as well as $A = 2$ (with enhancement, e.g. Millet et al., 2010). With waterside resistance reduced by half in the latter case, flux is

ACPD
14, 8015–8061, 2014

increased by ~ 20 % on average. This relative insensitivity is a result of the substantial airside resistance for acetaldehyde. We note that using the intrinsic Henry's solubility H and the total seawater acetaldehyde concentration in the flux estimation is incorrect on the basis that $C_a \neq C_w/H$ and $C_{a,0} \neq C_{w,0}/H$. As shown in Fig. 8c, inserting H in place of H^* overestimates acetaldehyde flux by about a factor of three. The effect of acetaldehyde chemical enhancement over the open ocean may be smaller still. According to the model of Hoover and Berkshire (1969), A approaches 2 only with a very rapid hydration rate (~ $3\,s^{-1}$) and at wind speeds of ~ $2\,m\,s^{-1}$; at $10\,m\,s^{-1}$ winds, A is reduced to ~ 1.4. At a slower hydration rate of ~ $0.1\,s^{-1}$, A is only ~ 1.1 in moderate winds.

Even with consideration of hydration, the agreement between measured and predicted flux is poor for acetaldehyde. The mean (standard error) EC flux is ~ 0.6 (0.2) $\mu mol\,m^{-2}\,d^{-1}$ for the entire transect, while at $A = 1$ the predicted flux is ~ 3 (0.2) $\mu mol\,m^{-2}\,d^{-1}$. When $A > 1$, the discrepancy between measured and predicted fluxes is even greater. The measurement was lower than expected possibly because the EC flux signal was close to the system's detection limit and not well resolved. The predicted flux could also be in error due to unknown biases in C_w and/or C_a. Decreasing C_w by ~ 2.5 nM or increasing C_a by ~ 0.15 ppb would bring predicted fluxes (A = 1) inline with observations. Crudely extrapolating EC and predicted acetaldehyde fluxes from the AMT-22 to the world oceans results in a mean (standard error) global air–sea transport of 3 (1) and 17 (1) $Tg\,yr^{-1}$, respectively. The predicted flux is similar to the estimate from Beale et al. (2013) of $17\,Tg\,yr^{-1}$. As with acetone, we could not derive the transfer velocity of acetaldehyde due to large uncertainties in the measurements. Future efforts on quantifying K_a of OVOCs should probably focus on the Northern Hemisphere, especially in continental outflow regions, where the flux signals and concentrations are large.

ACPD
14, 8015–8061, 2014

4.3 Methanol

As shown already by Yang et al. (2013b), the air–sea transfer velocity of methanol (K_{MeOH}) appears to resemble pure deposition (i.e. Flux $\approx -K_{MeOH}C_a$). As with k_{heat}, we use three different averaging approaches in the calculation of K_{MeOH} (= Flux/ $-C_a$) (Fig. 9): hourly flux divided by hourly ($-C_a$), bin-average of hourly K_{MeOH} according to wind speed (error bars correspond to 1α), and latitudinally averaged flux divided by latitudinally averaged ($-C_a$). Also shown is the estimate from the COARE model, which compares well with measurements up to wind speeds of $\sim 10\,m\,s^{-1}$. At higher winds, our limited number of measurements exceed the COARE estimate by up to $\sim 20\,\%$. We can further examine the validity of K_{MeOH} by comparing it to k_{heat}. In Fig. 10, latitudinal averages of K_{MeOH} (= Flux/ $-C_a$) are plotted against k_{heat} at neutral stability. K_{MeOH} is about 15 % lower than k_{heat} ($r^2 = 0.7$), consistent with the higher Sc_a for methanol (1.09) compared to heat (0.64). Using R_m from COARE and from Hicks et al. (1986), respectively, the expected ratios between these two transfer velocities are about 0.90 and 0.92. If the measured waterside concentration C_w were used in the K_{MeOH} calculation instead, the resultant K_{MeOH} would significantly exceed k_{heat}, as discussed in detail by Yang et al. (2013b).

The seawater concentrations of 15–62 nM observed during AMT-22 were much lower than previous observations (e.g. 48–361 nM during AMT-19 by Beale et al., 2013; about 60–230 nM by Williams et al., 2004 in the Tropical Atlantic). The reasons for this difference are currently unknown. Incubation experiments by Dixon et al. (2013) during AMT-19 indicated that there was significant in situ production and consumption of seawater methanol along the transect (net change ranging from −428 to +89 $nmol\,L^{-1}\,d^{-1}$). While primary production rates were lower during AMT-22 than during AMT-19 (G. Tilstone, AMT-22 Cruise Report), a direct linkage between phytoplankton production (and consumption) and dissolved methanol concentration has not been demonstrated.

The ratio between dissolved methanol concentrations at $\sim 500\,m$ and $\sim 5\,m$ was ~ 0.8 in the higher latitudes of the North Atlantic and ~ 0.6 elsewhere (Fig. 7),

ACPD
14, 8015–8061, 2014

proportionally similar to depth profiles measured previously by Williams et al. (2004) and Beale et al. (2013). Heikes et al. (2002) speculated the phytoplankton metabolite dimethylsulfoniopropionate (DMSP) to be a precursor of marine methanol. Near surface methanol concentrations from AMT-22 as well as AMT-19 (Beale et al., 2013) do not follow the previously measured trends in DMSP on AMT transects, which showed enhancement in productive waters relative to the oligotrophic gyres (Bell et al., 2010). At ~ 500 m, DMSP concentration should be essentially zero. Thus the source of dissolved methanol does not appear to be limited in the photic zone, which is consistent with a lack of diel difference in seawater methanol concentration during AMT-22 and also with the results from incubation experiments by Dixon et al. (2013).

4.4 Relationships between OVOCs and gross air–sea fluxes

We examine the relationships between the atmospheric OVOC concentrations south of 5° N, after the removal of the plastic funnel (Fig. 11). The high degrees of positive correlations between these compounds and their similar latitudinal distributions suggest that they share some common sources and sinks in the atmosphere (e.g. terrestrial emissions, photochemistry). In contrast, the relationships between OVOC concentrations were much weaker in the surface water (Fig. 12). This suggests that the oceanic budgets of these compounds may be dictated by different processes, such as biological production and consumption, photochemistry, atmospheric input, etc., the relative importance of which probably vary from gas to gas.

In global models of atmospheric OVOC cycling (e.g. Jacob et al., 2002; Heikes et al., 2002; Millet et al., 2008), air–sea transport is often separated into gross emission and deposition terms. This has the benefit of clearly distinguishing between the oceanic and atmospheric production/destruction pathways. The EC method yields net fluxes (i.e. the difference between the upwards and downwards fluxes). In Fig. 13, by setting C_a and C_w to zero, we calculate the gross emission and deposition fluxes for acetone, acetaldehyde, and methanol. The EC flux should lie within the bounds of the gross fluxes if the air/water concentrations and K_a in the flux prediction are reasonable.

ACPD
14, 8015–8061, 2014

For acetone, gross deposition (mean of $-6\,\mu mol\,m^{-2}\,d^{-1}$) and emission (mean of $7\,\mu mol\,m^{-2}\,d^{-1}$) mirror each other for most of the cruise track; the magnitudes of both terms are reduced in the South Atlantic, resulting in near zero net transport. For acetaldehyde, the predicted gross emission (mean of $5\,\mu mol\,m^{-2}\,d^{-1}$) exceeds deposition (mean of $-2\,\mu mol\,m^{-2}\,d^{-1}$), implying net emission. In the case of methanol, we use K_a ($=\mathrm{Flux}/-C_a$) from Yang et al. (2013b) instead of the predicted transfer velocity from the COARE model. Because of the low saturations of methanol (nominally $\sim 30\,\%$), the net methanol flux is fairly similar to the gross deposition flux, while the gross emission is small. The gross emission and depositions of the three OVOCs add up to be 15 and $-18\,\mu mol\,m^{-2}\,d^{-1}$, respectively. These are ~ 3 orders of magnitude smaller than the net air–sea gaseous TOC flux estimated by Dachs et al. (2005) in the Northeast Subtropical Atlantic, an area influenced by African outflow. To address the question of whether a substantial fraction of air–sea organic carbon is missing from the current species-specific estimates, a closure of the total air–sea gaseous organic carbon flux is urgently required.

5 Conclusion

On a trans-Atlantic cruise in 2012, we directly measured the air–sea fluxes of methanol, acetone, and acetaldehyde using a PTR-MS with the eddy covariance technique. We also measured their near surface concentrations, enabling a comparison between EC and predicted fluxes. Acetone flux was detected in the North Atlantic: the higher latitude waters represented a sink for acetone, while the subtropical gyre appeared to be a source. In the South Atlantic, measured acetone flux was near zero, as expected from the $\sim 100\,\%$ saturation in the near surface water. For acetaldehyde, the emission measured by EC was a few times smaller than expected based on measured concentrations and consideration of the hydration reaction. The transfer velocity of methanol correlated linearly with that of sensible heat, consistent with predominant airside controlled. Strong positive correlations were found between the atmospheric concentrations of

ACPD
14, 8015–8061, 2014

methanol, acetone, and acetaldehyde, suggesting similar sources and sinks of these compounds in air. Correlations in their seawater concentrations were much weaker, however, implying different oceanic production and destruction pathways.

Appendix A

Air–sea flux prediction

To compare with EC measurements, we compute the expected air–sea fluxes from the two-layer model (Liss and Slater, 1974):

$$\text{Flux} \approx K_a(C_w/H - C_a) \approx K_w(C_w - HC_a) \quad \text{(A1)}$$

The total gas transfer velocity can be written from the perspective of air concentration (K_a) as well as water concentration (K_w), which are related by the dimensionless liquid to gas solubility H: $K_a = HK_w$. C_w and C_a are the concentrations of the gas in water and air. A positive flux indicates sea-to-air emission.

The total gas transfer velocity may be partitioned to individual transfer velocities in the two phases (k_a and k_w, respectively):

$$K_a = 1/(1/k_a + 1/(AHk_w)) \quad \text{(A2)}$$

The term A accounts for chemical enhancement in waterside transfer due to aqueous hydration/reactions; A is assumed to be unity nonreactive gases such as methanol and acetone and has previously been estimated to be 2 for acetaldehyde due to hydration (see Sect. 4.2). Unlike sparingly soluble gases that are limited on the waterside (i.e. $K_w \approx k_w$), the exchange of highly soluble gases, such as methanol, is limited on the airside (i.e. $K_a \approx k_a$). For gases with intermediate solubility, such as acetone and acetaldehyde, resistances on the airside and the waterside are of similar magnitude such that the predicted flux is subject to combined uncertainties in k_a and k_w. From either

ACPD
14, 8015–8061, 2014

the airside or waterside perspective in Eq. (A1), zero concentration gradient is explicitly assumed in the other phase, which might lead to additional biases in the computed fluxes.

Unless otherwise specified, we use k_a and k_w from the COARE Gas Transfer model (Fairall et al., 2011) in the flux prediction. COARE accounts for turbulent and molecular diffusive resistance on the airside:

$$k_a = u_*/(R_t + R_m) \quad \text{(A3)}$$

The dimensionless turbulent (aerodynamic) resistance (R_t) is approximately equal to U/u_*. The molecular diffusive resistance is represented by $R_m = 13.3\mathrm{Sc}_a^{1/2}$, where Sc_a is the airside Schmidt number. In comparison, $R_m = 5\mathrm{Sc}_a^{2/3}$ from Hicks et al. (1986) is used in the parameterization of Duce et al. (1991). The essentially temperature-independent Sc_a is taken to be 1.09, 1.30 and 1.55 for methanol, acetaldehyde, and acetone, respectively (Johnson, 2010). To estimate k_w, the empirical constants for direct and bubble-mediated gas transfer are set to 1.3 (Blomquist et al., 2006) and 0 (due to the relatively high solubility of OVOCs, Woolf, 1997), respectively. In the predictions of sensible heat and water vapor transfer, fits to historical measurements of dimensionless transfer coefficients (C_h and C_e) are used in COARE (e.g. $k_{heat} = C_h U$).

A survey of published solubility values (Sander, 1999) suggests uncertainties of 10–20 % at 25 °C for OVOCs; additional uncertainties exist in the temperature and salinity dependence of solubility. For acetone and acetaldehyde, we use the solubility measured in seawater by Zhou and Mopper (1990). For the latter, the reported solubility includes aqueous hydration. For methanol, we use the solubility in freshwater from Snider and Dawson (1985) and neglect its weak salinity dependence owning to the small molecular size (Johnson, 2010). To relate the airside and waterside, latidudinally averaged atmospheric measurements are linearly interpolated to the times of water collection.

ACPD
14, 8015–8061, 2014

Appendix B

OVOC backgrounds

Backgrounds for OVOC air measurements ($bkgd_{air}$) were quantified by directing ambient air through a platinum catalytic converter (Shimadzu) for 2 min at the beginning of every hour. Heated to 350 °C, the converter should oxidize organic compounds to CO_2 but not significantly alter the oxygen and water signals. At about 0.076 % of the O_2^+ signal in air, the oxygen isotope ($^{16}O^{17}O^+$) accounted for about half of the m/z 33 background in air measurements. As documented by Beale et al. (2011), the seawater background ($bkgd_{water}$) was taken to be the PTR-MS response when measuring the carrier flow (high purity nitrogen gas passing through a separate but identical catalytic converter) that bypassed the silicone membrane.

Comparing $bkgd_{air}$ with $bkgd_{water}$, for acetone the two values were within ~ 10 %, implying a high efficiency of the catalyst at removing this compound. For methanol, the two backgrounds were also similar after accounting for the contribution of $^{16}O^{17}O^+$ in air. For acetaldehyde, however, $bkgd_{air}$ was 0.03–0.15 ppb (mean of 0.09 ppb) higher than $bkgd_{water}$. Furthermore, this discrepancy became greater when the atmospheric acetaldehyde concentration was higher, suggesting that the catalyst was less efficient at removing m/z 45. We thus use $bkgd_{water}$ to calculate the atmospheric acetaldehyde concentrations. This analysis suggests that the atmospheric acetaldehyde concentrations reported by Yang et al. (2013a) at a coastal site, which were computed based on $bkgd_{air}$, may be underestimated by ~ 0.1 ppb.

ACPD
14, 8015–8061, 2014

Appendix C

Motion-sensitivity in EC fluxes

Methanol flux demonstrates a motion-sensitivity in large swell. In Fig. C1, the averaged variance spectra of methanol and acetone over ∼ 10 h on 13 November are shown, when wind speeds were about 16 m s^{-1} and the vertical platform variance over 2 m^2 s^{-2}. An unexpected peak can be seen in the raw methanol spectrum between 0.1 and 0.2 Hz (the frequency of ship's motion), which manifest as positive/negative peaks in the corresponding methanol : w cospectrum. This artifact was not observed in the raw acetone spectrum. Further analysis yielded spurious correlations between the atmospheric methanol concentration and vertical ship acceleration as well as displacement.

The correlation between methanol concentration and acceleration was a motion-induced artifact with the PTR-MS. In heavy seas, the source water vapor flow, nominally steady, fluctuated by up to ∼ 0.5 sccm around the set value of 9.0 sccm, leading to sinusoidal variations in the O_2^+ signal. This motion-sensitivity propagated to m/z 33 in the form of $^{16}O^{17}O^+$, increasing the apparent variability of the methanol signal. In contrast, acetone concentration and ship's motion did not significantly correlate. The correlation of methanol concentration with platform displacement may be due to vertical heaving of the ship across a concentration gradient. From similarity theory, Yang et al. (2013b) estimated an average vertical gradient of 0.002 ppb m^{-1} for methanol within the surface layer of the atmosphere. In heavy seas, the bow of the ship may heave with a 10 m amplitude and thus induce an apparent variation of 0.02 ppb, which would represent ∼ 14 % of the observed σ at a dwell time of 200 ms. Blomquist et al. (2010) showed a worst-case error of 18 % in the measured air–sea flux in an analysis of dimethylsulfide due to this motion gradient effect. Acetone concentration did not correlate with platform displacement during this period, likely because the saturation of acetone was ∼ 100 % (i.e. no vertical concentration gradient).

ACPD
14, 8015–8061, 2014

To address these artifacts, we decorrelate the atmospheric methanol concentration with the ship's vertical acceleration and displacement. This effectively removed the artificial peaks in the variance and covariance spectra between 0.1–0.2 Hz while preserving the signal at other frequencies. The corrected methanol : w cospectrum is reasonably fitted by the theoretical Kaimal spectrum. The decorrelation reduced the magnitude of the methanol flux by 2.5 $\mu mol\, m^{-2}\, d^{-1}$ (24 %) on average for the entire AMT-22 cruise. In heavy seas (vertical platform variance $> 2\, m^2\, s^{-2}$), the reduction in flux was up to 10 $\mu mol\, m^{-2}\, d^{-1}$. We apply an analogous decorrelation to T_a from the sonic anemometer, which is also subject to the motion gradient effect but should be insensitive to the ship's acceleration. Decorrelation reduces the magnitude of the sensible heat flux by only a few percent in heavy seas, confirming that most of the motion-related artifact in methanol flux was related to the PTR-MS.

Appendix D

Funnel-induced artifacts in acetaldehyde and acetone flux

Contamination from the plastic funnel, if uncorrelated with the vertical wind velocity, in theory should not affect the EC flux. However, artifacts are apparent in the acetaldehyde and acetone cospectra at frequencies over ~ 0.1 Hz in the Northern Hemisphere (e.g. Fig. 3). Contamination from the funnel may have varied with the airflow through the inlet as well as the resultant temperature fluctuation. In the tropical North Atlantic and under strong sunlight, we observed greater emissions from the funnel when the ship was stationary than when the ship was underway, presumably due to changes in the relative wind speeds (and so cooling rates). Decorrelation of acetone and acetaldehyde concentrations with ship's motion proved ineffective at removing these artifacts, forcing us to discard fluxes when the cospectra were severely distorted in the Northern Hemisphere (i.e 24–28 October for acetone).

ACPD
14, 8015–8061, 2014

Appendix E

Potential contribution to OVOC fluxes due to density fluctuations

Temperature and pressure are precisely controlled in the PTR-MS, while the long inlet tubing likely dampens most of the water vapor flux. Thus a "Webb" correction (Webb et al., 1980) should not be necessary. Nevertheless, it is instructive to examine the magnitude of the potential contribution from density fluctuations to EC flux. From in situ meteorological and surface ocean data, the COARE model predicts a mean vertical wind velocity ($\overline{w}$) of -1.0×10^{-4} to 3.9×10^{-4} m s^{-1} (mean of 0.9×10^{-4} m s^{-1}) for the entire cruise. Multiplying $\overline{w}$ by the atmospheric methanol concentration leads to a mean (maximum) apparent flux of 0.13 (0.57) µmol m^{-2} d^{-1}, which is ~ 2 orders of magnitude lower than the observed flux and in the opposite direction. For acetaldehyde and acetone, because of their lower atmospheric concentrations the "Webb" terms are even smaller.

Acknowledgements. This work is supported by the United States National Science Foundation (Grant no. OISE-1064405) and the PML Kingsland Fellowship. The AMT cruise is supported by the UK Natural Environment Research Council National Capability funding to Plymouth Marine Laboratory and the National Oceanography Centre, Southampton. This is a contribution to the international SOLAS and IMBER projects and represents contribution number 245 of the AMT program. The first author would like to thank P. Mason, A. Staff, and S. Howell for instrumentation support, J. Stephens and F. Hopkins for equipment set up, T. Bell, and J. Dixon for scientific input, and finally B. Huebert and C. Fairall for continued guidance.

References

Bariteau, L., Helmig, D., Fairall, C. W., Hare, J. E., Hueber, J., and Lang, E. K.: Determination of oceanic ozone deposition by ship-borne eddy covariance flux measurements, Atmos. Meas. Tech., 3, 441–455, doi:10.5194/amt-3-441-2010, 2010.

ACPD
14, 8015–8061, 2014

Beale, R., Dixon, J., Liss, P., and Nightingale, P.: Quantification of oxygenated volatile organic compounds in seawater by membrane inlet-proton transfer reaction/mass spectrometry, Anal. Chim. Acta, 706, 128–134, 2011.
Beale, R., Dixon, J., Arnold, S., Liss, P., and Nightingale, P.: Methanol, acetaldehyde and acetone in the surface waters of the Atlantic Ocean, J. Geophys. Res., 18, 5412–5425, doi:10.1002/jgrc.20322, 2013.
Bell, R. P. and Avans, P. G.: Kinetics of the dehydration of methylene glycol in aqueous solution, Proc. R. Soc. Lon. Ser.-A, 291, 297–321, 1966.
Bell, R. P., Rand, M. H., and Wynne-Jones, K. M. A.: Kinetics of the hydration of acetaldehyde, Trans. Faraday Soc., 52, 1093–1102, 1956.
Bell, T. G., Poulton, A. J., and Malin, G.: Strong linkages between dimethylsulphoniopropionate (DMSP) and phytoplankton community physiology in a large subtropical and tropical Atlantic Ocean data set, Global Biogeochem. Cy., 24, GB3009, doi:10.1029/2009GB003617, 2010.
Benkelberg, H. J., Hamm, S., and Warneck, P.: Henry's low coefficients for aqueous solutions of acetone, acetaldehyde and acetonitrile, equilibrium constants for the addition-compounds of acetone and acetaldehyde with bisulfite, J. Atmos. Chem., 20, 17–34, 1995.
Blomquist, B., Fairall, C. W., Huebert, B. J., Kieber, D., and Westby, G.: DMS seaair transfer velocity: direct measurements by eddy covariance and parameterization based on the NOAA/COARE gas transfer model, Geophys. Res. Lett., 33, L07601, doi:10.1029/2006GL025735, 2006.
Blomquist, B. W., Huebert, B. J., Fairall, C. W., and Faloona, I. C.: Determining the sea–air flux of dimethylsulfide by eddy correlation using mass spectrometry, Atmos. Meas. Tech., 3, 1–20, doi:10.5194/amt-3-1-2010, 2010.
Carpenter, L. J., Lewis, A. C., Hopkins, J. R., Read, K. A., Longley, I. D., and Gallagher, M. W.: Uptake of methanol to the North Atlantic Ocean surface, Global Biogeochem. Cy., 18, GB4027, doi:10.1029/2004GB002294, 2004.
Carpenter, L. J., Archer, S. D., and Beale, R.: Ocean-atmosphere trace gas exchange, Chem. Soc. Rev., 41, 6473–6506, 2012.
Dachs, J., Calleja, M. L., Duarte, C. M., del Vento, S., Turpin, B., Polidori, A., Herndl, G. J., and Agustì, S.: High atmosphere–ocean exchange of organic carbon in the NE subtropical Atlantic, Geophys. Res. Lett., 32, L21807, doi:10.1029/2005GL023799, 2005.
Dixon, J. L., Beale, R., and Nightingale, P. D.: Production of methanol, acetaldehyde, and acetone in the Atlantic Ocean, Geophys. Res. Lett., 40, 1–6, doi:10.1002/grl.50922, 2013.

ACPD
14, 8015–8061, 2014

Duce, R. A., Liss, P. S., Merrill, J. T., Atlas, E. L., Buat-Menard, P., Hicks, B. B., Miller, J. M., Prospero, J. M., Arimoto, R., Church, T. M., Ellis, W., Galloway, J. N., Hansen, L., Jickells, T. D., Knap, A. H., Reinhardt, K. H., Schneider, B., Soudine, A., Tokos, J. J., Tsunogai, S., Wollast, R., and Zhou, M.: The atmospheric input of trace species to the World Ocean, Global Biogeochem. Cy., 5, 193–259, 1991.

Edson, J., Hinton, A., Prada, K., Hare, J., and Fairall, C.: Direct covariance flux estimates from mobile platforms at sea, J. Atmos. Ocean. Tech., 15, 547–562, 1998.

Fairall, C. W., Bradley, E. F., Rogers, D. P., Edson, J. B., and Yong, G. S.: Bulk parameterization of air–sea fluxes for Tropical Ocean–Global Atmosphere Coupled-Ocean Atmosphere response experiment, J. Geophys. Res., 101, 3747–3764, 1996.

Fairall, C. W., Yang, M., Bariteau, L., Edson, J. B., Helmig, D., McGillis, W., Pezoa, S., Hare, J. E., Huebert, B., and Blomquist, B.: Implementation of the Coupled Ocean-Atmosphere Response Experiment flux algorithm with CO_2, dimethyl sulfide, and O_3, J. Geophys. Res., 116, C00F09, doi:10.1029/2010JC006884, 2011.

Fischer, E. V., Jacob, D. J., Millet, D. B., Yantosca, R. M., and Mao, J.: The role of the ocean in the global atmospheric budget of acetone, Geophys. Res. Lett., 39, L01807, doi:10.1029/2011GL050086, 2012.

Guenther, A., Geron, C., Pierce, T., Lamb, B., Harley, P., and Fall, R.: Natural emissions of non-methane volatile organic compounds; carbon monoxide, and oxides of nitrogen from North America, Atmos. Environ., 34, 2205–2230, 2000.

Heald, C. L., Goldstein, A. H., Allan, J. D., Aiken, A. C., Apel, E., Atlas, E. L., Baker, A. K., Bates, T. S., Beyersdorf, A. J., Blake, D. R., Campos, T., Coe, H., Crounse, J. D., DeCarlo, P. F., de Gouw, J. A., Dunlea, E. J., Flocke, F. M., Fried, A., Goldan, P., Griffin, R. J., Herndon, S. C., Holloway, J. S., Holzinger, R., Jimenez, J. L., Junkermann, W., Kuster, W. C., Lewis, A. C., Meinardi, S., Millet, D. B., Onasch, T., Polidori, A., Quinn, P. K., Riemer, D. D., Roberts, J. M., Salcedo, D., Sive, B., Swanson, A. L., Talbot, R., Warneke, C., Weber, R. J., Weibring, P., Wennberg, P. O., Worsnop, D. R., Wittig, A. E., Zhang, R., Zheng, J., and Zheng, W.: Total observed organic carbon (TOOC) in the atmosphere: a synthesis of North American observations, Atmos. Chem. Phys., 8, 2007–2025, doi:10.5194/acp-8-2007-2008, 2008.

Heikes, B. G., Chang, W. N., Pilson, M. E. Q., Swift, E., Singh, H. B., Guenther, A., Jacob, D. J., Field, B. D., Fall, R., Riemer, D., and Brand, L.: Atmospheric methanol budget and ocean implication, Global Biogeochem. Cy., 16, 1133, doi:10.1029/2002GB001895, 2002.

ACPD
14, 8015–8061, 2014

Hicks, B., Wesely, M., Lindberg, S., and Bromberg, S.: Proceedings of the NAPAP Workshop on Dry Deposition, Harpers Ferry, W. Va., 25–27 March, p. 77 1986.
Hoover, T. E. and Berkshire, D. C.: Effects of hydration on carbon dioxide exchange across an air–water interface, J. Geophys. Res., 74, 456–464, 1969.
Jacob, D. J., Field, B. D., Jin, E. M., Bey, I., Li, Q., Logan, J. A., Yantosca, R. M., and Singh, H. B.: Atmospheric budget of acetone, J. Geophys. Res., 107, 4100, doi:10.1029/2001JD000694, 2002.
Jacob, D. J., Field, B. D., Li, Q. B., Blake, D. R., de Gouw, J., Warneke, C., Hansel, A., Wisthaler, A., Singh, H. B., and Guenther, A.: Global budget of methanol: constraints from atmospheric observations, J. Geophys. Res., 110, D08303, doi:10.1029/2004JD005172, 2005.
Johnson, M. T.: A numerical scheme to calculate temperature and salinity dependent air-water transfer velocities for any gas, Ocean Sci., 6, 913–932, doi:10.5194/os-6-913-2010, 2010.
Jardine, K., Harley, P., Karl, T., Guenther, A., Lerdau, M., and Mak, J. E.: Plant physiological and environmental controls over the exchange of acetaldehyde between forest canopies and the atmosphere, Biogeosciences, 5, 1559–1572, doi:10.5194/bg-5-1559-2008, 2008.
Kaimal, J., Wyngaard, J., Izumi, Y., and Coté, O.: Spectral characteristics of surface layer turbulence, Q. J. Roy. Meteor. Soc., 98, 563–589, doi:10.1002/qj.49709841707, 1972.
Kameyama, S., Tanimoto, H., Inomata, S., Tsunogai, U., Ooki, A., Takeda, S., Obata, H., Tsuda, A., and Uematsu, M.: High-resolution measurement of multiple volatile organic compounds dissolved in seawater using equilibrator inlet-proton transfer reaction-mass spectrometry (EI-PTR-MS), Mar. Chem., 122, 59–73, 2010.
Karl, T., Guenther, A., Lindinger, C., Jordan, A., Fall, R., and Lindinger, W.: Eddy covariance measurements of oxygenated volatile organic compound fluxes from crop harvesting using a redesigned proton-transfer-reaction mass spectrometer, J. Geophys. Res., 106, 24157–24167, doi:10.1029/2000JD000112, 2001.
Karl, T., Potosnak, M., Guenther, A., Clark, D., Walker, J., Herrick, J. D., and Geron, C.: Exchange processes of volatile organic compounds above a tropical rain forest: implications for modeling tropospheric chemistry above dense vegetation, J. Geophys. Res., 109, D18306, doi:10.1029/2004JD004738, 2004.
Kieber, R. J., Zhou, X., and Mopper, K.: Formation of carbonyl compounds from UV-induced photodegradation of humic substances in natural waters: fate of riverine carbon in the sea, Limnol. Oceanogr., 35, 1503–1515, 1990.

ACPD
14, 8015–8061, 2014

Kurz, J. L. and Coburn, J. I.: The hydration of acetaldehyde, II. Transition-state characterization, J. Am. Chem. Soc., 89, 3524–3528, 1967.
Lerot, C., Stavrakou, T., De Smedt, I., Müller, J.-F., and Van Roozendael, M.: Glyoxal vertical columns from GOME-2 backscattered light measurements and comparisons with a global model, Atmos. Chem. Phys., 10, 12059–12072, doi:10.5194/acp-10-12059-2010, 2010.
Lewis, A. C., Hopkins, J. R., Carpenter, L. J., Stanton, J., Read, K. A., and Pilling, M. J.: Sources and sinks of acetone, methanol, and acetaldehyde in North Atlantic marine air, Atmos. Chem. Phys., 5, 1963–1974, doi:10.5194/acp-5-1963-2005, 2005.
Lindinger, W., Hansel, A., and Jordan, A.: On-line monitoring of volatile organic compounds at pptv levels by means of Proton-Transfer-Reaction Mass Spectrometry (PTR-MS), medical applications, food control and environmental research, Int. J. Mass Spectrom., 173, 191–241, 1998.
Liss, P. S. and Slater, P. G.: Flux of gases across the airsea interface, Nature, 247, 181–184, doi:10.1038/247181a0, 1974.
Marandino, C. A., De Bruyn, W. J., Miller, S. D., Prather, M. J., and Saltzman, E. S.: Oceanic uptake and the global atmospheric acetone budget, Geophys. Res. Lett., 32, L15806, doi:10.1029/2005GL023285, 2005.
Millet, D. B., Jacob, D. J., Turquety, S., Hudman, R. C., Wu, S., Fried, A., Walega, J., Heikes, B. G., Blake, D. R., Singh, H. B., Anderson, B. E., and Clarke, A. D.: Formaldehyde distribution over North America: implications for satellite retrievals of formaldehyde columns and isoprene emission, J. Geophys. Res., 111, D24S02, doi:10.1029/2005JD006853, 2006.
Millet, D. B., Jacob, D. J., Custer, T. G., de Gouw, J. A., Goldstein, A. H., Karl, T., Singh, H. B., Sive, B. C., Talbot, R. W., Warneke, C., and Williams, J.: New constraints on terrestrial and oceanic sources of atmospheric methanol, Atmos. Chem. Phys., 8, 6887–6905, doi:10.5194/acp-8-6887-2008, 2008.
Mopper, K. and Kieber, D. J.: Distribution and biological turnover of dissolved organic compounds in the water column of the Black Sea, Deep-Sea Res., 38, 1021–1047, 1991.
Read, K., Carpenter, L., Arnold, S., Beale, R., Nightingale, P., Hopkins, J., Lewis, A., Lee, J., Mendes, L., and Pickering, S.: Multiannual observations of acetone, methanol, and acetaldehyde in remote tropical Atlantic air: implications for atmospheric OVOC budgets and oxidative capacity, Environ. Sci. Technol., 46, 11028–11039, 2012.

ACPD
14, 8015–8061, 2014

Sander, R.: Compilation of Henry's Law constants for inorganic and organic species of potential importance in environmental chemistry (Version 3), available at: http://www.henrys-law.org (last access: 19 March 2014), 1999.

Schecker, H. and Schultz, G.: Untersuchungen zur Hydrationskinetik von Formaldehyd in wässriger Lösung, Z. Phys. Chem. Neue Fol., 65, 221–224, 1969.

Singh, J., Chen, Y., Tabazadeh, A., Fukui, Y., Bey, I., Yantosca, R., Jacob, D., Arnold, F., Wohlfrom, K., Atlas, E., Flocke, F., Blake, D., Blake, N., Heikes, B., Snow, J., Talbot, R., Gregory, G., Sachse, G., Vay, S., and Kondo, Y.: Distribution and fate of selected oxygenated organic species in the troposphere and lower stratosphere over the Atlantic, J. Geophys. Res., 105, 3795–3805, 2000.

Singh, H. B., Tabazadeh, A., Evans, M. J., Field, B. D., Jacob, D. J., Sachse, G., Crawford, J. H., Shetter, R., and Brune, W. H.: Oxygenated volatile organic chemicals in the oceans: inferences and implications based on atmospheric observations and air–sea exchange models, Geophys. Res. Lett., 30, 1862, doi:10.1029/2003GL017933, 2003.

Singh, H. B., Salas, L. J., Chatfield, R. B., Czech, E., Fried, A., Walega, J., Evans, M. J., Field, B. D., Jacob, D. J., Blake, D., Heikes, B., Talbot, R., Sachse, G., Crawford, J. H., Avery, M. A., Sandholm, S., and Fuelberg, H.: Analysis of the atmospheric distribution, sources, and sinks of oxygenated volatile organic chemicals based on measurements over the Pacific during TRACE-P, J. Geophys. Res., 109, D15S07, doi:10.1029/2003JD003883, 2004.

Sinreich, R., Coburn, S., Dix, B., and Volkamer, R.: Ship-based detection of glyoxal over the remote tropical Pacific Ocean, Atmos. Chem. Phys., 10, 11359–11371, doi:10.5194/acp-10-11359-2010, 2010.

Snider, J. and Dawson, G.: Tropospheric light alcohols, carbonyls, and acetonitrile: concentrations in the southwestern United States and Henry's law data, J. Geophys. Res., 90, 3797–3805, 1985.

Spirig, C., Neftel, A., Ammann, C., Dommen, J., Grabmer, W., Thielmann, A., Schaub, A., Beauchamp, J., Wisthaler, A., and Hansel, A.: Eddy covariance flux measurements of biogenic VOCs during ECHO 2003 using proton transfer reaction mass spectrometry, Atmos. Chem. Phys., 5, 465–481, doi:10.5194/acp-5-465-2005, 2005.

Stavrakou, T., Müller, J.-F., De Smedt, I., Van Roozendael, M., Kanakidou, M., Vrekoussis, M., Wittrock, F., Richter, A., and Burrows, J. P.: The continental source of glyoxal estimated by the synergistic use of spaceborne measurements and inverse modelling, Atmos. Chem. Phys., 9, 8431–8446, doi:10.5194/acp-9-8431-2009, 2009.

ACPD
14, 8015–8061, 2014

Taddei, S., Toscano, P., Gioli, B., Matese, A., Miglietta, F., Vaccari, F. P., Zaldei, A., Custer, T., and Williams, J.: Carbon dioxide and acetone air–sea fluxes over the Southern Atlantic, Environ. Sci. Technol., 43, 5218–5222, 2009.

Webb, E. D., Pearman, G. I., and Leuning, R.: Correction of flux measurements for density due to heat and water vapor transport, Q. J. Roy. Meteor. Soc., 106, 85–100, doi:10.1002/qj.49710644707, 1980.

Williams, J., Holzinger, R., Gros, V., Xu, X., Atlas, E., and Wallace, D. W. R.: Measurements of organic species in air and seawater from the tropical Atlantic, Geophys. Res. Lett., 31, L23S06, doi:10.1029/2004GL020012, 2004.

Woolf, D. K.: Bubbles and their role in gas exchange, in: The Sea Surface and Global Change, edited by: Duce, R. and Liss, P., Cambridge Univ. Press, New York, 173–205, doi:10.1017/CBO9780511525025.007, 1997.

Wróblewski, T., Ziemczonek, L., Alhasan, A. M., and Karwasz, G. P.: Ab initio and density functional theory calculations of proton affinities for volatile organic compounds, Eur. Phys. J.-Spec. Top., 144, 191–195, doi:10.1140/epjst/e2007-00126-7, 2007.

Yang, M., Beale, R., Smyth, T., and Blomquist, B.: Measurements of OVOC fluxes by eddy covariance using a proton-transfer-reaction mass spectrometer – method development at a coastal site, Atmos. Chem. Phys., 13, 6165–6184, doi:10.5194/acp-13-6165-2013, 2013a.

Yang, M., Nightingale, P., Beale, R., Liss, P., Blomquist, B., and Fairall, C.: Atmospheric deposition of methanol over the Atlantic Ocean, Proc. Natl. Acad. Sci. USA, 110, 20034–20039, doi:10.1073/pnas.1317840110, 2013b.

Zhao, J. and Zhang, R. Y.: Proton transfer reaction rate constants between hydronium ion (H_3O^+) and volatile organic compounds, Atmos. Environ., 38, 2177–2185, 2004.

Zhou, X. and Mopper, K.: Apparent partition coefficients of 15 carbonyl compounds between air and seawater and between air and freshwater; implications for air–sea exchange, Environ. Sci. Technol., 24, 1864–1869, 1990.

Zhou, X. and Mopper, K.: Photochemical production of low-molecular-weight carbonyl compounds in seawater and surface microlayer and their air–sea exchange, Mar. Chem., 56, 201–213, 1997.

ACPD
14, 8015–8061, 2014

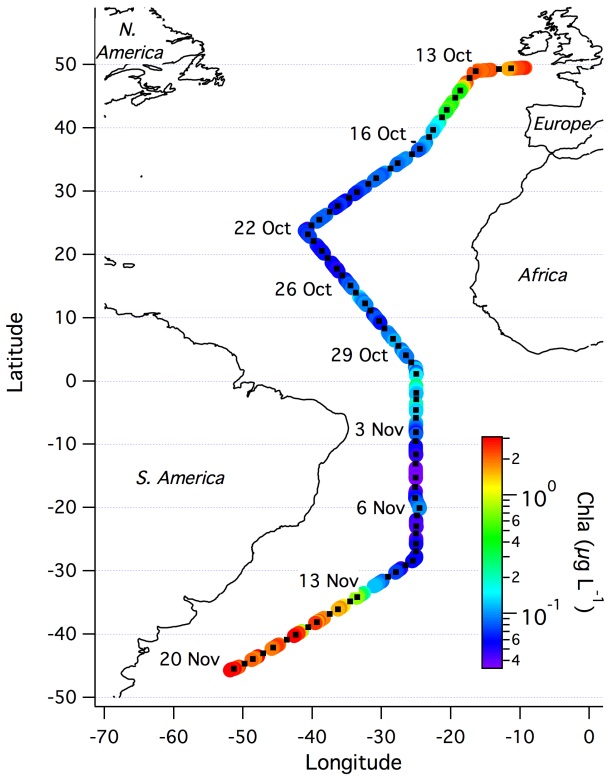

Fig. 1. Cruise track of AMT-22 color-coded by chlorophyll *a* concentration and marked on selected dates. The black squares indicate the locations of CTD casts.

ACPD
14, 8015–8061, 2014

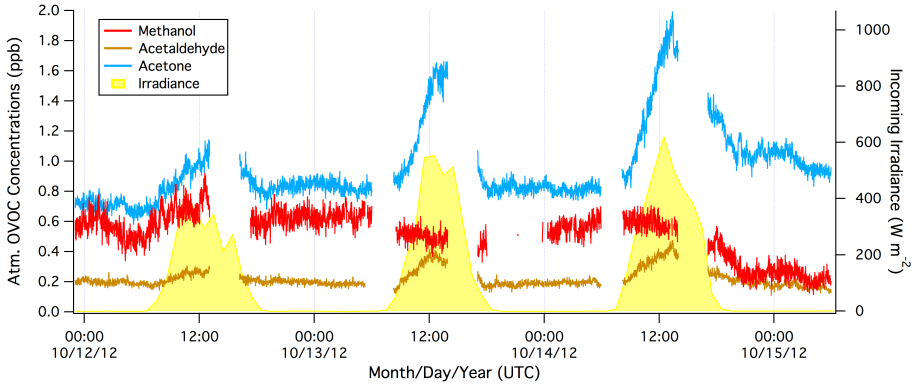

Fig. 2. An example of contamination in the acetaldehyde and acetone signals due to outgassing from a plastic funnel at the front of the inlet. The artifact was the most severe under direct sunlight and at high temperatures, leading to unrealistic diurnal cycles. Methanol was not affected. This contamination disappeared immediately after the removal of the plastic funnel on 29 October.

ACPD
14, 8015–8061, 2014

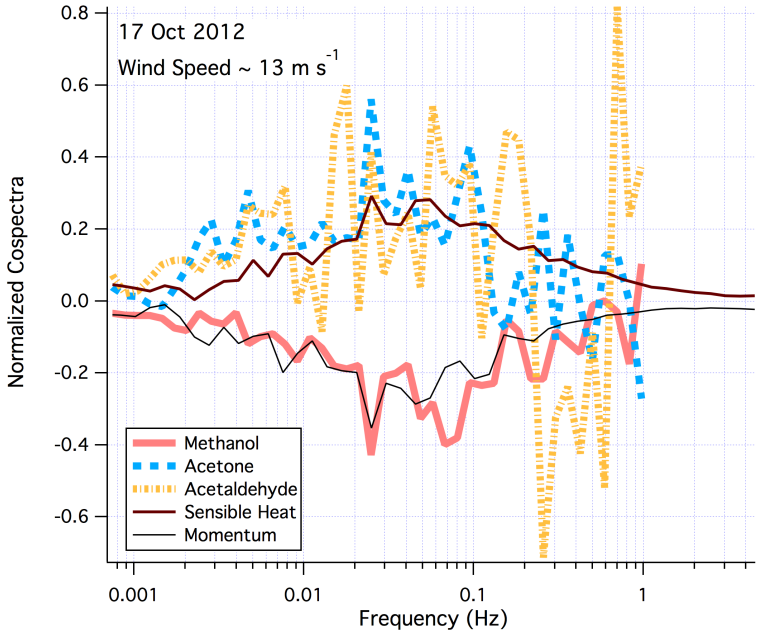

Fig. 3. Cospectra of methanol, acetone, acetaldehyde, sensible heat and momentum with the vertical wind velocity on a day of high winds. Each cospectrum is normalized to the respective flux magnitude. Cospectra of heat, momentum, and methanol followed the expected spectral shape, while those of acetone and acetaldehyde were distorted at frequencies above 0.1 Hz, likely due to contamination from the plastic funnel.

ACPD
14, 8015–8061, 2014

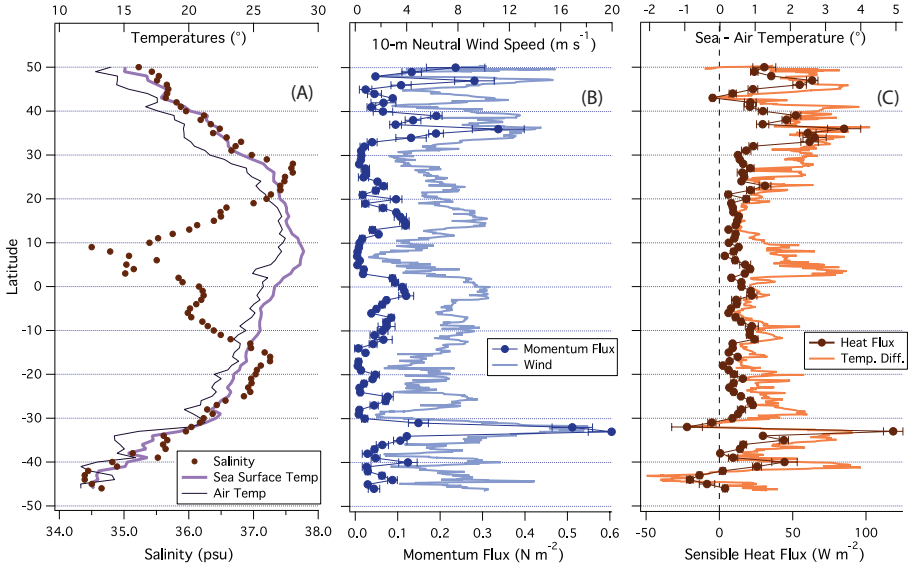

Fig. 4. (A) Sea surface temperature, air temperature, and salinity **(B)** wind speed and momentum flux; **(C)** air–sea temperature difference and sensible heat flux. Sensible heat flux was usually from sea-to-air, except for short periods preceding storms near the beginning and end of the cruise. Error bars on fluxes correspond to standard errors.

ACPD
14, 8015–8061, 2014

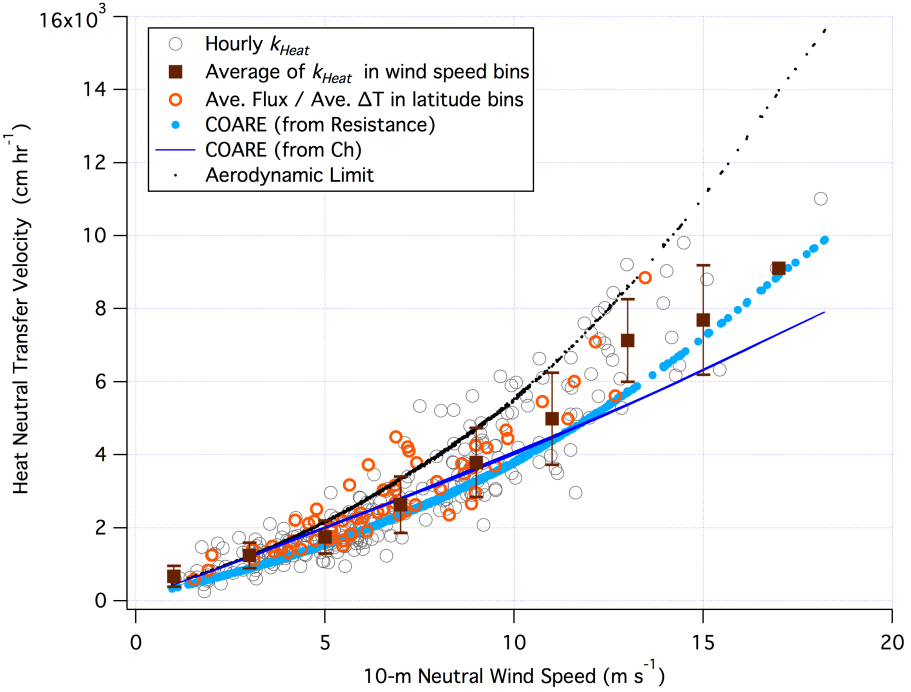

Fig. 5. Measured heat transfer velocity vs. wind speed. Three approaches of data averaging are shown (see text for details). For clarity, only hours when $\Delta T > 1\,^{\circ}C$ and relative wind direction between −30 and 100° are shown. Error bars indicate standard deviations from the bin averages. Two parameterizations of heat transfer from the COARE model as well as the aerodynamic limit are also shown.

ACPD
14, 8015–8061, 2014

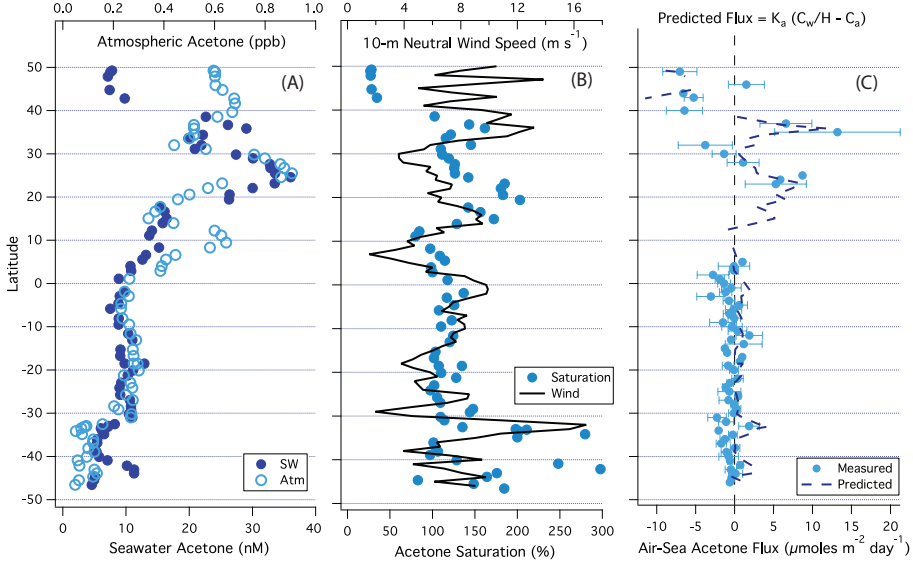

Fig. 6. (A) Atmospheric and seawater (~ 5 m depth) concentrations of acetone; **(B)** saturation of acetone and wind speed; **(C)** flux measured by EC and predicted with the two-layer model.

ACPD
14, 8015–8061, 2014

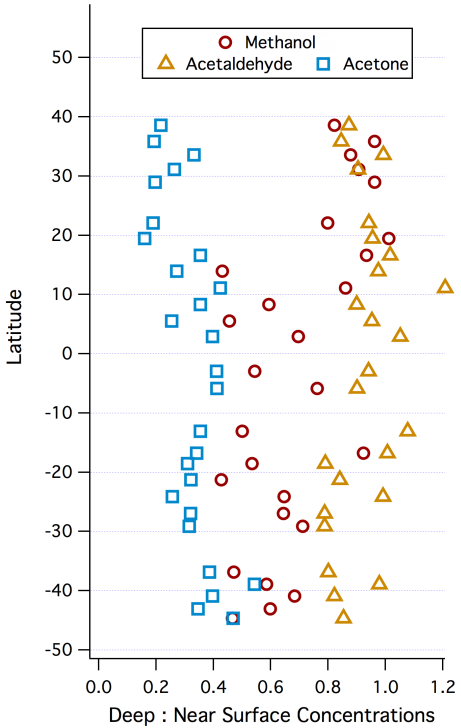

Fig. 7. Ratios of seawater OVOC concentrations from depth (nominally 500 m) to those from ~ 5 m. For methanol, this ratio was ~ 0.8 in the North Atlantic and ~ 0.6 elsewhere. For acetaldehyde, concentrations at depth were similar to concentrations near the surface. Acetone concentration showed the most reduction at depth, with a fraction ranging from ~ 0.2 in the subtropical North Atlantic to ~ 0.4 in the higher latitudes of the South Atlantic.

ACPD
14, 8015–8061, 2014

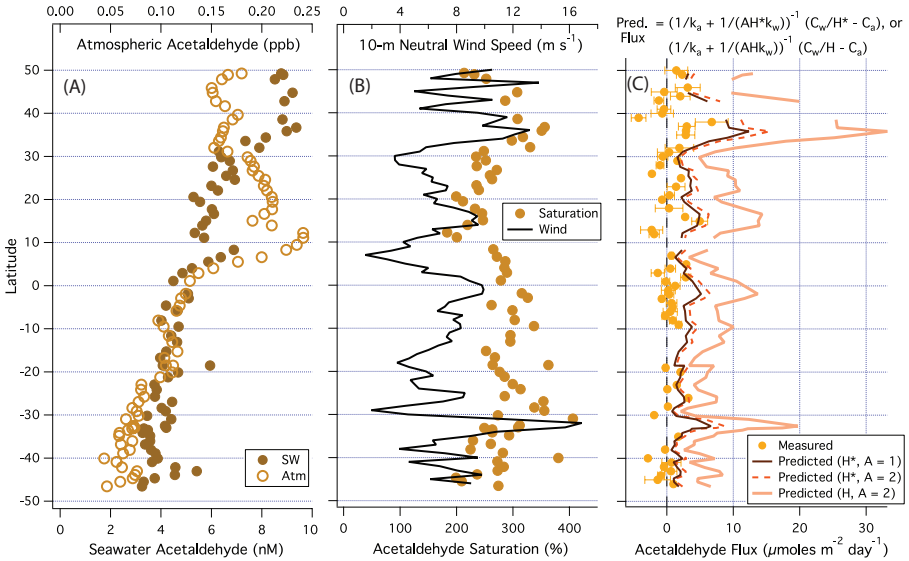

Fig. 8. (A) Atmospheric and seawater (~ 5 m depth) concentrations of acetaldehyde; **(B)** saturation of acetaldehyde and wind speed; **(C)** flux measured by EC and predicted with the two-layer model with three different considerations of hydration/chemical enhancement.

ACPD
14, 8015–8061, 2014

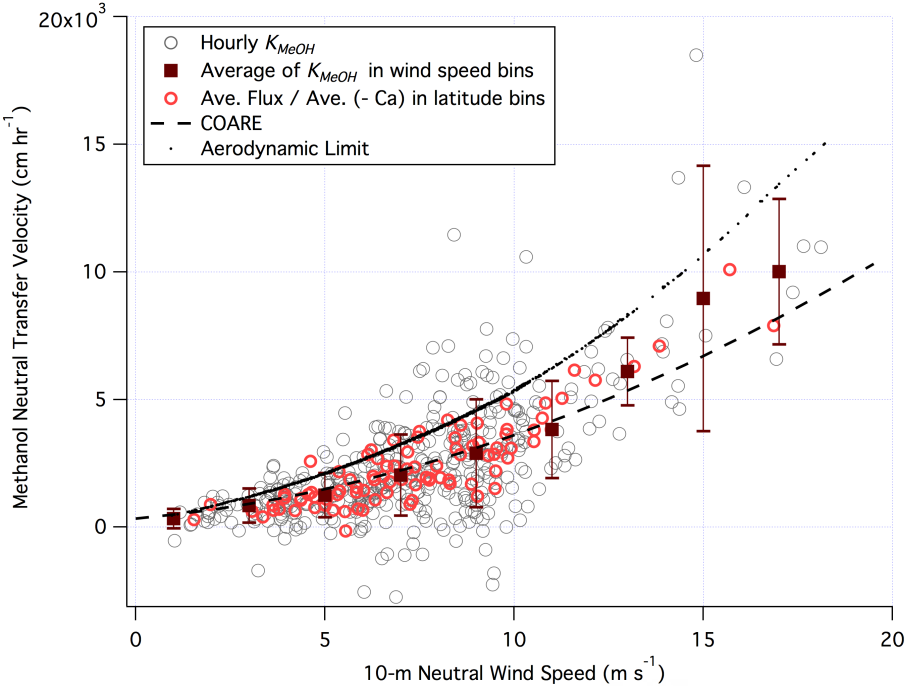

Fig. 9. Transfer velocity of methanol calculated with a purely depositional approach vs. wind speed. Three types of averaging are shown (see text for details). Error bars correspond to standard deviations from the bin averages. Measured methanol transfer velocity is up to ~ 20 % greater than the COARE estimate in high winds. The aerodynamic limit describes the rate of turbulent transfer in the atmosphere.

ACPD
14, 8015–8061, 2014

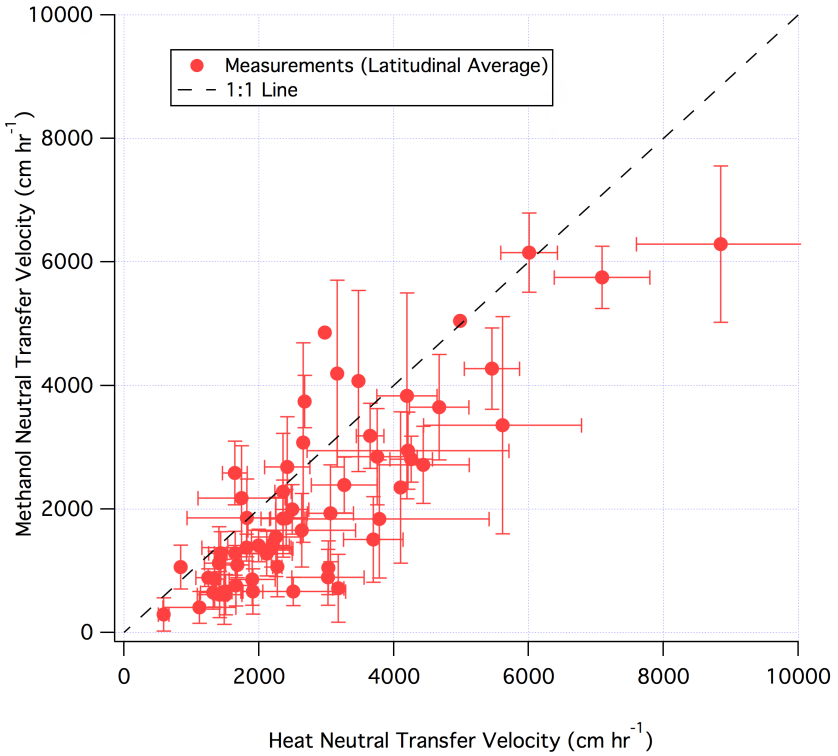

Fig. 10. Methanol transfer velocity vs. heat transfer velocity in latitudinal bins (error bars indicate standard errors). Methanol transfer velocity was ~ 85 % of the heat transfer velocity, consistent with the lower diffusivity (higher Schmidt number) of methanol than heat in air.

ACPD
14, 8015–8061, 2014

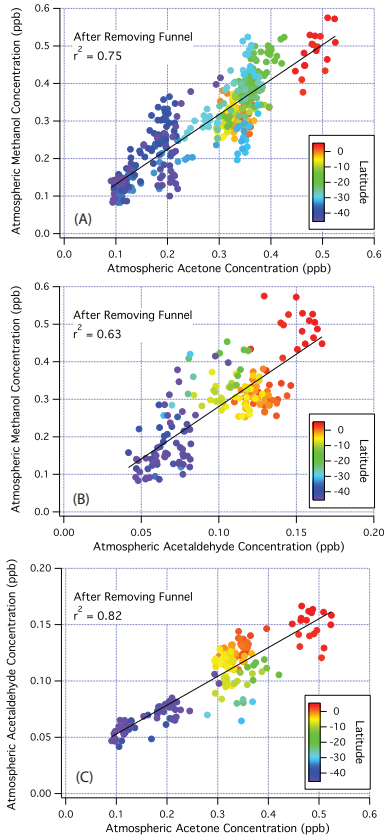

Fig. 11. Atmospheric concentrations of **(A)** methanol vs. acetone, **(B)** methanol vs. acetaldehyde, and **(C)** acetaldehyde vs. acetone after the removal of the inlet funnel, color-coded by latitude. The high degrees of positive correlations between these compounds and their similar latitudinal distributions imply that they share some common sources and sinks.

ACPD
14, 8015–8061, 2014

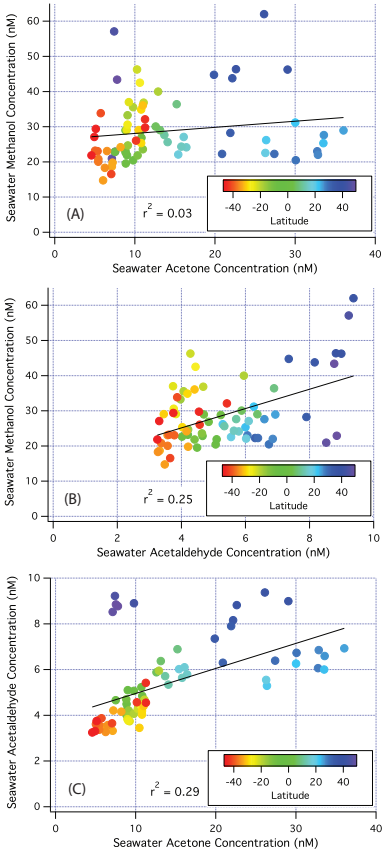

Fig. 12. Near surface seawater concentrations of **(A)** methanol vs. acetone, **(B)** methanol vs. acetaldehyde, and **(C)** acetaldehyde vs. acetone, color-coded by latitude. Correlations between seawater concentrations are much lower than those between air concentrations, implying different oceanic production and consumption pathways of these compounds.

ACPD
14, 8015–8061, 2014

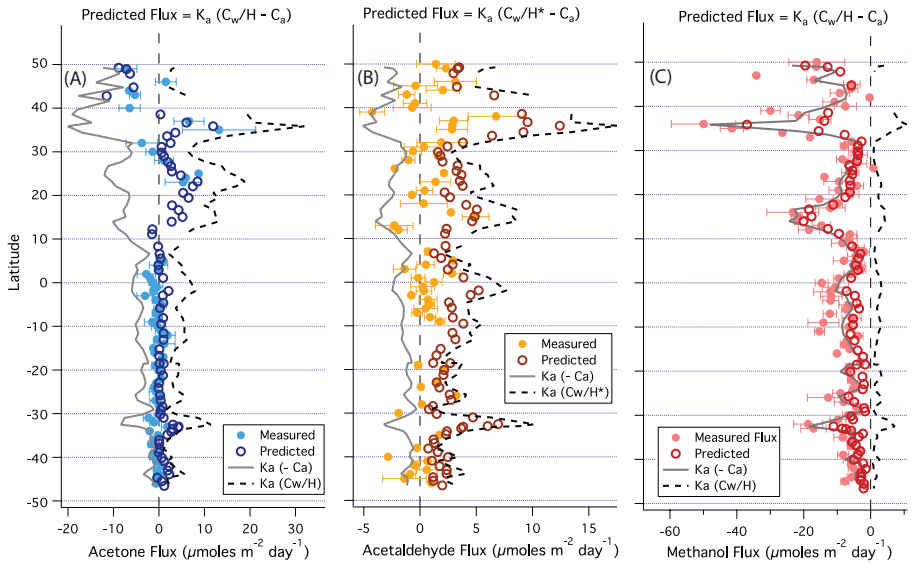

Fig. 13. Measured as well as predicted net (difference between emission and deposition) and gross (total emission and deposition) fluxes for acetone, acetaldehyde, and methanol.

ACPD
14, 8015–8061, 2014

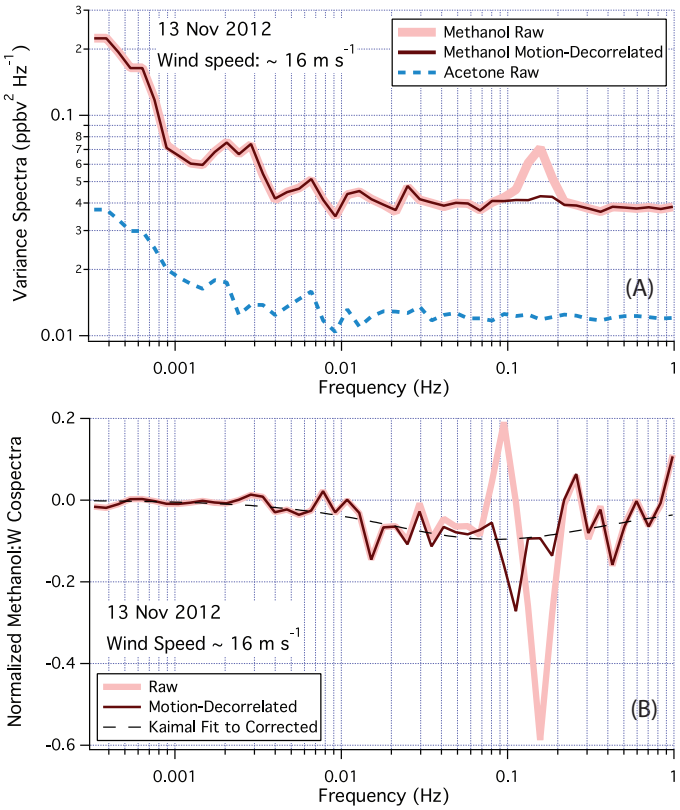

Fig. C1. (A) Variance spectra of methanol (raw and motion-decorrelated) and acetone (raw) averaged over 10 h on a day of high winds and severe motion; **(B)** cospectra of methanol : *w* (raw and motion-decorrelated) on this date. Decorrelation effectively removes the artificial peak in the raw methanol variance spectrum at the frequency of ship's motion (0.08–0.2 Hz), while preserving the spectrum elsewhere. The corrected methanol cospectrum is reasonably described by a Kaimal fit.

ACPD
14, 8015–8061, 2014